Physics 441, Lab 4:
Alpha-Induced X-ray Emission

Joseph Wilson Yazuardi, Yufeng Chen
(Dated: June 23, 2025)

X-ray spectroscopy was performed using an alpha-induced emission setup to calibrate and analyze a series of known and unknown material samples. Energy calibration was performed using copper and titanium samples, where their K_{α_1} and K_{β_1} transition peaks were fitted to a linear fit. Known materials such as aluminum, nickel, a U.S. quarter, and a YBCO superconductor were measured to validate our calibration. The aluminum sample yielded a clear K_{α_1} peak at (1.57 ± 0.13) keV, and an unexpected secondary peak at (6.4 ± 0.5) keV, attributed to the iron metal source holder. The U.S. quarter yielded copper and nickel peaks that qualitatively agree with the theoretical percent composition by gross area and intensity. The YBCO superconductor sample yielded multiple peak transitions from barium, copper, and yttrium, with the exception of oxygen due to low detection. Moseley's Law was validated using measured K_{α_1} and K_{β_1} transitions from known materials, yielding experimental gradients of 0.098 ± 0.005 and 0.11 ± 0.02 respectively. One unknown yielded tantalum as a major element with L_{α_1} and L_{β_1} peaks at (8.1±0.8) keV and (9.3±0.9) keV. The other yielded elemental lead and bismuth at their respective L-series transitions. Minor peaks across all samples were observed but excluded due to insufficient signal strength or the lack of corresponding pairs for confident elemental identification. Nevertheless, the consistent agreement between measured and theoretical values and validation of Moseley's Law demonstrates the accuracy, reliability, and effectiveness of X-ray spectroscopy in elemental identification.

I. INTRODUCTION

X-ray spectroscopy is a reliable and widely used technique for identifying the elemental composition of materials by analyzing the energies of emitted X-ray photons. These emissions occur when high-energy particles eject inner-shell electrons, allowing electrons from higher energy levels to transition downward and release energy. Like a fingerprint, each element has its own unique set of characteristic X-ray lines, making this method valuable in applications such as materials analysis and industrial research. This technique relies on Moseley's Law, which describes a linear relationship between the square root of the X-ray energy and the atomic number of the element. We aim to validate the accuracy and reliability of this law by measuring the K_α and K_β transitions of several known elements. We will also identify the composition of known samples by analyzing the selected peaks in their spectra and comparing them with theoretical predictions, to assess how accurately this method performs. A particular focus is placed on YBCO ($YBa_2Cu_3O_7$), a high-temperature superconductor with a complex multi-element structure. This structure gives the material its unique superconducting properties, which are useful in many applications such as medical physics. The presence of multiple elements makes YBCO an ideal case for testing the limitations of X-ray spectroscopy, especially for detecting lighter elements like oxygen, which often fall below the detector's sensitivity. The experiment is conducted using an alpha-induced X-ray emission setup and a multi-channel analyzer system for spectral data collection. Calibration is performed using titanium and copper samples. Overall, this experiment is performed to verify Moseley's Law and test the effectiveness of X-ray spectroscopy in elemental identification.

II. EXPERIMENTAL SETUP AND DATA COLLECTION

A. Experimental Diagram

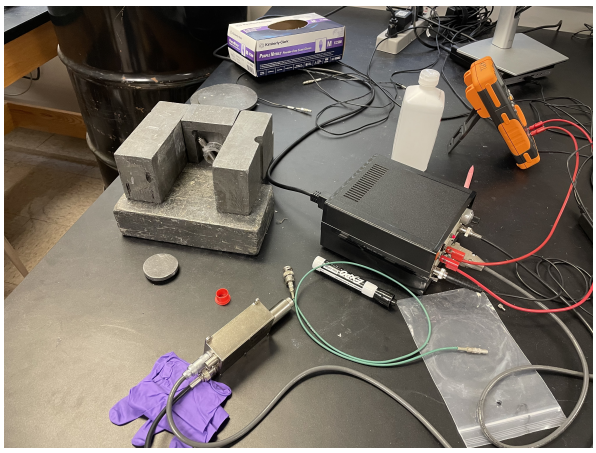

FIG. 1. Experimental setup for X-ray spectroscopy, consisting of a Cm-244 alpha source to induce characteristic X-ray emissions from target samples, a cooled silicon PiN diode detector (Amptek XR-100CR) to convert incident X-rays into charge pulses, a PX2CR preamplifier and shaping amplifier to condition the signal, and a multi-channel analyzer (MCA8000A) that digitizes the signal and interfaces with the MCA software for spectral acquisition and analysis [1].

B. Calibration of the X-Ray Energy Scale

Before analyzing our unknown and known samples, the calibration of the energy scale of the detector must be performed. The apparatus does not have a pre-calibrated assignment between the MCA channel numbers and photon energies. Therefore, we must establish a linear fit energy calibration using samples with known characteristic X-ray emission lines. Copper (Cu) and titanium (Ti) samples, are utilized as they emit well-characterized K_{α_1} and K_{β_1} transitions when bombarded by alpha particles. These characteristic X-rays correspond to electronic transitions from higher atomic shells to the $n = 1$ (K-shell) level. The energy values for these transitions are referenced from the standard "Characteristic X-Ray Energies" table [2], and will be assigned to the observed peak positions in the spectrum.

For the calibration, we assign the measured channel numbers of the K_{α_1} and $K_{\beta_1}$for Cu and Ti with their known X-ray energies. The assigned data is then fitted to yield a linear relation of the form:

$$E = A + B \cdot C, \tag{1}$$

where E is the photon energy in keV, C is the MCA channel number, and A and B are the intercept and slope of the calibrated curve, respectively.

C. Elemental Identification from Known samples

To validate the accuracy and reliability of our calibrated apparatus, we will first test four known samples: nickel (Ni), aluminum (Al), a U.S. quarter coin, and a YBCO superconducting disk. Upon exposure to alpha particles from the Cm-244 source, the inner-shell electrons in these elements are ejected, resulting in electronic transitions that emit characteristic X-rays. For most cases, we expect to observe K_{α_1} and K_{β_1} transitions, corresponding to electron transitions into the $n = 1$ shell (K-shell) or from $n = 2$ and $n = 3$, respectively. However, if the K-shell binding energy of an element is more than what the incident energy can excite, then the L_α and L_β transitions may dominate instead. The calibrated spectra for each element were analyzed to obtain the energy values of the selected peaks, and compared to the theoretical values of the respective transitions from [2]. We expect to see a close agreement between observed and theoretical values to validate our calibration and the accuracy and reliability of the apparatus.

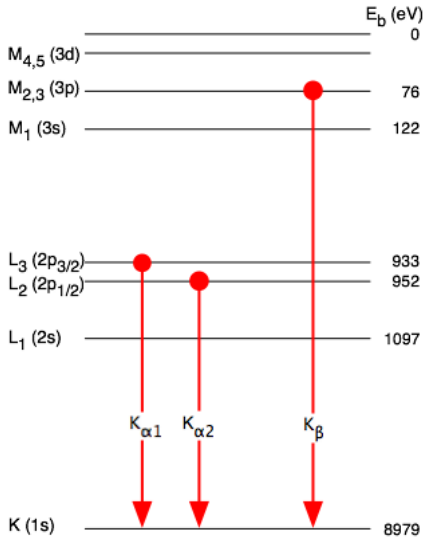

FIG. 2. Energy level diagram showing the electronic transitions for the K_{α_1}, K_{α_2}, and K_β X-ray emission lines in copper. The K_{α_1} and K_{α_2} lines originate from transitions from the L_3 $(2p_{3/2})$ and L_2 $(2p_{1/2})$ levels to the K-shell. This diagram helps visualize the characteristic peaks observed in the spectra of known and unknown samples. Adapted from [3].

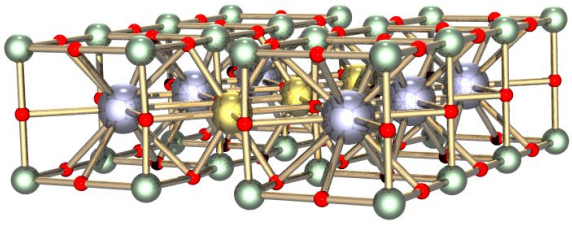

FIG. 3. Crystal structure of $YBa_2Cu_3O_7$ (YBCO), a high-temperature superconductor. The structure contains several different elements arranged in layers and as barium, yttrium, copper, and oxygen are all in different parts of the structure, the bonding becomes complex. This makes it hard to get an accurate analysis of the full composition using X-ray spectroscopy especially as oxygen produces a weak signal that's below our detector's range. Adapted from [4].

D. Verification of Moseley's Law

Plots of Moseley's Law will be made for both the K_α and K_β transition energies to validate the accuracy of Moseley's Law. The energy of characteristic X-ray lines can be expressed as:

$$E = E_0(Z - s)^2 \left(\frac{1}{n_f^2} - \frac{1}{n_i^2} \right), \tag{2}$$

where E is the emitted X-ray energy, E_0 is the Rydberg energy at 13.6 eV, Z is the atomic number, s is the

screening constant, and n_i, n_f are the principal quantum numbers of the initial and final states, respectively. The principal quantum numbers for K_{α_1} are $n_f = 1$ and $n_i = 2$ for K_α . On the other hand, $n_f = 1$ and $n_i = 3$ for K_{β_1}.

The expressions for the characteristic energy simplifies to:

$$E_{K\alpha} = \frac{3}{4}E_0(Z-s)^2, \tag{3}$$

$$E_{K\beta} = \frac{8}{9}E_0(Z-s)^2. \tag{4}$$

Taking the square root of both expressions yields a linear relation:

$$\sqrt{E_{K\alpha}} = \sqrt{\frac{3}{4}E_0} \cdot (Z-s), \tag{5}$$

$$\sqrt{E_{K\beta}} = \sqrt{\frac{8}{9}E_0} \cdot (Z-s). \tag{6}$$

This corresponds to the general linear equation:

$$\sqrt{E} = mZ + c, \tag{7}$$

where m is the gradient and c is the intercept.

The uncertainty for linear regression programmed with Python:

$$\sigma = \sqrt{\text{pcov}[0,0]}, \tag{8}$$

where pcov is the covariance matrix returned by the fitting function.

By comparing the experimentally determined slope with our theoretical prediction, we can determine the accuracy and reliability of our measurements across multiple samples. As our plot uses energy in keV units, the theoretical gradients become $\sqrt{0.0102} \approx 0.101$ for K_α transitions and $\sqrt{0.0121} \approx 0.110$ for K_β transitions.

E. Elemental Identification from Unknown Samples

After validating the accuracy and reliability of the apparatus and detector using known samples, we are able to analyze 2 unknown samples to observe the major elemental composition. The determination of peaks and transitions is more tedious and interpretive as there is no prior knowledge of the sample's composition. We aim on focusing on the major peaks in the spectrum, as these are more probable to correspond to the more dominant elements within an unknown sample. Minor peaks were also observed but were not analyzed, as they do not provide enough information for confident elemental identification. This approach allows us to infer the composition of the unknown sample without making false assumptions about less prominent elements. The elemental identification process lies on the assumption that the most intense peaks correspond to the most abundant elements in the material.

III. PRESENTATION & ANALYSIS OF DATA

A. Calibration of the X-ray Energy Scale.

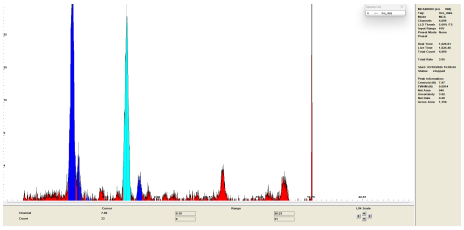

FIG. 4. Calibration spectrum using the copper and titanium sample. The theoretical K_{α_1} and K_{β_1} peaks for copper (8.05 keV and 8.91 keV) and titanium (4.51 keV and 4.93 keV) were assigned to their corresponding MCA channel numbers. These values were obtained directly from the standard X-ray emission table [2] and used to construct a linear calibration curve. A linear fit was applied to define the energy scale for subsequent trials.

B. Elemental Identification from Known Samples

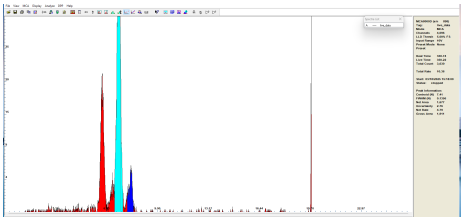

FIG. 5. Spectrum of the nickel sample. The experimental K_{α_1} and K_{β_1} peaks for copper are (7.4 ± 0.8) keV and (8.2 ± 0.8) keV respectively, which is consistent with our theoretical expectations. A third minor peak can be observed but is not analyzed due to its weak intensity and potential interference from background noise, reflecting the resolution limits of the apparatus.

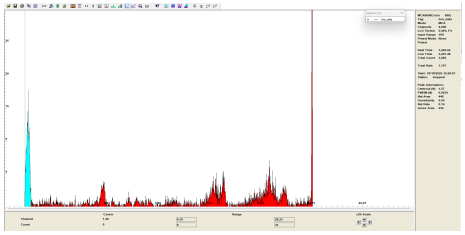

FIG. 6. Spectrum of the aluminum sample. The experimental K_{α_1} peak for alumnium is (1.57 ± 0.13) keV, which is consistent with our theoretical predictions. No distinct K_{β_1} peak is observed, likely due to the low X-ray count rate from the aluminum sample. A second visible peak is observed at (6.4±0.5) keV addoes not correspond to any known aluminum transition. It is assumed to be the secondary emission from surrounding samples such as the metal sample holder.

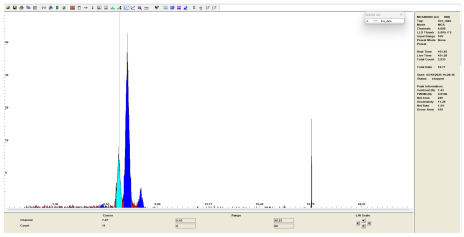

FIG. 7. Spectrum of the U.S. quarter coin sample. The first experimental peak corresponds to the K_{α_1} transition of nickel at (7.4 ± 0.7). The second and third peaks correspond to the K_{α_1} transition of copper at (8.0±0.8) keV and K_{β_1} transition of copper at (8.8 ± 0.8) keV respectively. The K_{β_1} transition of nickel is not analyzed in this spectrum, possibly due to an overlap with copper peaks or a lower relative abundance within the sample.

Based on the U.S. Mint specifications [5], the theoretical percent composition of a modern U.S. quarter is:

$$\text{Cu} = 91.67\%$$
$$\text{Ni} = 8.33\%$$

From our X-ray spectrum of the quarter, we observed and analyzed the K_{α_1} transitions of both copper and nickel peaks. The intensity and gross area of the copper peak is significantly larger than the nickel peak, indicating that copper is indeed the dominant element in the sample. While our analysis does not yield the exact percent composition, this qualitative analysis supports the expected composition and our theoretical predictions.

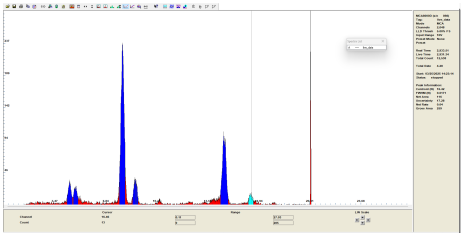

FIG. 8. Spectrum of the YBCO superconductor. The first experimental two peaks correspond to the L_{α_1} and L_{β_1} transitions of barium at (4.5±0.4) keV and (4.9±0.4) keV respectively. The middle two peaks correspond to the K_{α_1} and K_{β_1} transitions of copper at (7.9 ± 0.8) keV and (8.8 ± 0.8) keV respectively. The last two peaks correspond to the K_{α_1} and K_{β_1} transitions of Yttrium at (14.7±1.4) keV and (16.4±1.5) keV respectively. Peaks corresponding to the transitions of oxygen is not observed, as its characteristic energy lies below the detector's sensitivity range and the count rate is too low to be detected.

Using the theoretical mass composition values provided by WebQC [6], the expected elemental breakdown of YBCO is:

$$\text{Y} = 13.16\%$$
$$\text{Ba} = 40.72\%$$
$$\text{Cu} = 27.33\%$$
$$\text{O} = 18.80\%$$

While a full percent composition analysis is tedious due to the complex structure of YBCO and limitations in detecting light elements like oxygen, we only will relatively compare the major peaks. From our observations and analysis on the K_{α_1} and K_{β_1} transitions, the copper peak is approximately twice the intensity and gross area of the yttrium peak, which is consistent with the theoretical mass composition values where copper accounts for 27.33% and yttrium for 13.16% of the total mass. However, it is more accurate to compare the relative number of atoms per unit cells over the mass. Barium is not utilized for our comparison as it undergoes L_{α_1} and L_{β_1} transitions. Our results help to validate our identification of the major components in the material without a full percent composition analysis.

C. Verification of Moseley's Law

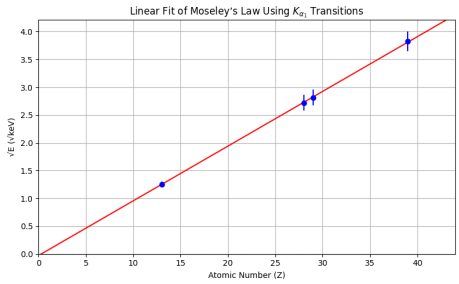

FIG. 9. Linear fit of $\sqrt{E}$ versus atomic number Z using measured K_{α_1} transition energies. The resulting fit, $\sqrt{E} = (0.098 \pm 0.005)Z + (-0.03 \pm 0.11)$, has a gradient of 0.098 which aligns closely with the theoretical gradient of 0.101, validating the theory of Moseley's Law.

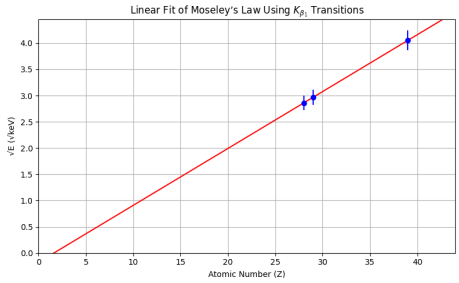

FIG. 10. Linear fit of $\sqrt{E}$ versus atomic number Z using measured K_{β_1} transition energies. The resulting fit, $\sqrt{E} = (0.11 \pm 0.02)Z + (-0.2 \pm 0.6)$, has a gradient of 0.11 which aligns closely with the theoretical gradient of 0.110. The slope is steeper than that of the K_{α_1} fit which validates Moseley's Law. Aluminum was excluded from this fit due to the secondary emission from surrounding materials such as the metal sample holder.

D. Elemental Identification from Unknown Samples

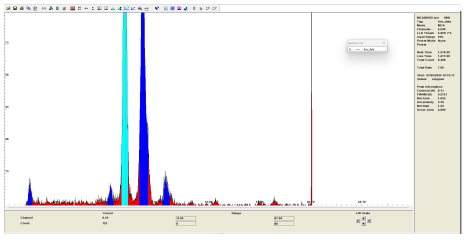

FIG. 11. X-ray spectrum showing two dominant peaks, identified as the L_{α_1} and L_{β_1} transitions of Tantalum (Ta) at (8.1 ± 0.8) keV and (9.3 ± 0.9) keV. Our experimental values are close to the theoretical values from [2] and minor peaks were excluded as they lacked a corresponding pair for elemental identification.

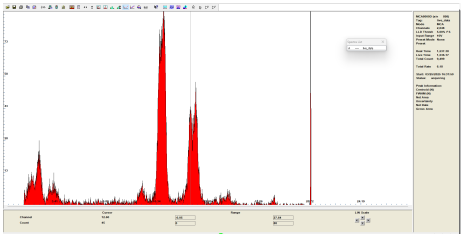

FIG. 12. X-ray spectrum with four major peaks identified as the L_{α_1} and L_{β_1} transitions of both Lead (Pb) and Bismuth (Bi). Lead (Pb) is identified at (10.50 ± 1.0) keV and (12.60 ± 1.3) keV and Bismuth (Bi) is identified at (10.80 ± 1.0) keV and (12.99 ± 1.3) keV. Our experimental values are close to the theoretical values from [2] and minor peaks were excluded as they lacked a corresponding pair for elemental identification.

IV. DISCUSSION AND CONCLUSION

Our observations and analysis in this experiment successfully demonstrated the principles of X-ray spectroscopy and its application in elemental identification. Our experimental results generally agree with our theoretical predictions as we faced certain issues in our analysis. The interference of background noise and insufficient detection of a transition peak by the detector requires attention from our instructors and confident peak identification and assignment. A proper calibration was performed using titanium and copper samples to produce a best-fitted energy scale for the MCA detector system. The accuracy and reliability of our calibration was verified using known samples before testing unknown samples. We expect to observe and analyze the K_{α_1} and K_{β_1} transitions in the peaks yielded. However, if the K-shell binding energy of an element is more than what the incident energy can excite, then the L_α and L_β transitions may dominate instead.

The observations and analysis of known samples such as aluminum, nickel, YBCO superconductor, and a U.S. quarter confirmed that our calibration was accurate and reliable. Aluminum showed a clear K_{α_1} transition peak at (1.57 ± 0.13) keV, consistent with the theoretical peak of 1.4867 keV. A second peak at (6.4 ± 0.5) keV was attributed to the secondary emission from surrounding materials such as the metal sample holder. This is likely the element iron, which has a theoretical K_{α_1} transition peak of 6.404 keV. The nickel sample yielded K_{α_1} and K_{β_1} peaks at (7.4 ± 0.8) keV and (8.2 ± 0.8) keV, respectively, which is in good agreement with the theoretical peak of 7.478 keV and 8.265 keV. The U.S. quarter coin spectrum yielded a K_{α_1} transition peak at (7.4 ± 0.7) keV for nickel, and K_{α_1} and K_{β_1} transitions for copper at (8.0 ± 0.8) keV and (8.8 ± 0.8) keV, respectively. These values agree with the theoretical values of 7.478 keV (Ni), 8.047 keV (Cu K_{α_1}), and 8.905 keV (Cu K_{β_1}). The quarter coin, being an alloy of 91.67% Cu and 8.33% Ni [5], is designed and manufactured for better durability and resistance to corrosion. Our qualitative analysis using gross area and intensity effectively validated the comparison,

supporting the reliability of our experimental technique and the experiment.

YBCO ($YBa_2Cu_3O_7$) is a high-temperature superconductor that introduced a complex analysis due to its multi-element and complex structure. It showed clear peaks for barium with L_{α_1} at (4.5 ± 0.4) keV and L_{β_1} at (4.9 ± 0.4) keV, copper with K_{α_1} at (7.9 ± 0.8) keV and K_{β_1} at (8.8 ± 0.8) keV, and yttrium with K_{α_1} at (14.7 ± 1.4) keV and K_{β_1} at (16.4 ± 1.5) keV. These experimental values align with the theoretical values of 4.465 keV (Ba L_{α_1}), 4.828 keV (Ba L_{β_1}), 8.047 keV (Cu K_{α_1}), 8.905 keV (Cu K_{β_1}), 14.958 keV (Y K_{α_1}), and 16.738 keV (Y K_{β_1}). The copper peak was observed to be approximately twice the intensity of the yttrium peak, consistent with the theoretical mass composition of 27.33% Cu and 13.16% Y [6]. Oxygen, which comprises 18.80% of the mass composition, could not be detected as its characteristic energy lies below the detector's sensitivity range and the count rate is too low to be detected. YBCO's layered structure and multiple oxidation states make it a complex material to possess unique superconducting properties. Its role as a superconductor in magnetic levitation and power transmission shows the importance of superconductors and our observations into it.

Moseley's Law was validated by plotting the K_{α_1} and K_{β_1} transitions in a linear best-fit. In both transitions, we observed an excellent agreement between $\sqrt{E}$ and atomic number Z, with gradients of 0.098 ± 0.005 and 0.11 ± 0.02. These values agrees well with the theoretical values of $\sqrt{0.0102} \approx 0.101$ and $\sqrt{0.0121} \approx 0.110$, respectively. Our results validated our expectations of the accuracy and reliability of Moseley's Law and our experiment.

After known samples were utilized to validate the accuracy and reliability of our apparatus, two unknown samples were utilized to further our insight into X-ray spectroscopy. The first unknown sample yielded two major peaks with L_{α_1} at (8.1 ± 0.8) keV and L_{β_1} at (9.3 ± 0.9) keV, which correspond to the transitions of tantalum (Ta). Minor peaks can be observed but are not taken into account as they do not have yield enough information for an accurate and reliable elemental identification. Tantalum is heavily researched on as it has a high melting point and high corrosion resistance, which are valuable traits in the aerospace and electronics. The second unknown sample is more complex and yielded four peaks with L_{α_1} at (10.50 ± 1.0) keV and L_{β_1} at (12.60 ± 1.3) keV for lead (Pb), and L_{α_1} at (10.80 ± 1.0) keV and L_{β_1} at (12.99 ± 1.3) keV for bismuth (Bi). These agrees with their respective theoretical values from [2] and validates the presence of both elements in the sample. Lead (Pb) and Bismuth (Bi) are commonly combined as a coolant in certain nuclear reactors and gross peak area analysis with intensity showed that both were major elements. Although there are other minor peaks, they were not analyzed as they lacked a corresponding pair for a accurate and reliable elemental identification.

In conclusion, this experiment validated Moseley's Law, confirmed the accuracy and reliability of our calibration, and demonstrated the capability of X-ray spectroscopy to analyze both simple and complex samples. There were a lot of issues faced as expected in a experimental setting and with the guide of the instructors and lab experience, the confident selection of peaks and elemental identification along with the disregard of background noises and anomalies was made possible. The study and analysis of standard metals, industrial alloys, and a superconductor like YBCO highlighted the versatility of the X-ray spectroscopy method for elemental identification analysis in physics and engineering.

[1] University of Michigan Physics Department. X-ray spectroscopy laboratory manual. University of Michigan, Ann Arbor, 2005. Physics 441-442, Advanced Physics Laboratory.

[2] J. A. Bearden. X-ray wavelengths. *Reviews of Modern Physics*, 39(1):78–124, 1967.

[3] Gert. Why is k-alpha (3/2) always more intense than k-alpha (1/2) in copper? https://physics.stackexchange.com/questions/398724/why-is-k-alpha-3-2-always-more-intense-than-k-alpha-1-2-in-copper, 2018. Physics Stack Exchange, accessed 2025-03-31.

[4] Wikipedia contributors. Yttrium barium copper oxide. `https://en.wikipedia.org/wiki/Yttrium_barium_copper_oxide`, 2024. Accessed: 2025-03-31.

[5] United States Mint. Coin specifications. `https://www.usmint.gov/learn/coins-and-medals/circulating-coins/coin-specifications`, 2024. Accessed 2025-03-31.

[6] WebQC. Molecular weight of yba_2cu_3o_7. `https://www.webqc.org/molecular-weight-of-YBa2Cu3O7.html`, 2024. Accessed: 2025-03-31.